Modeling triangular titration fronts in the O_2+H_2 reaction on a catalytic Rh(111) surface

Michael Monine and Len Pismen[a)]
Department of Chemical Engineering, Technion, 32000 Technion City, Haifa, Israel

Markus Bär and Michal Or-Guil
Max-Planck-Institut für Physik komplexer Systeme, Nöthnitzer Str. 38, 01187 Dresden, Germany

(Received 2 January 2002; accepted 4 June 2002)

We present a model for the titration of an oxygen saturated catalytic Rh(111) surface with hydrogen. Oxygen is removed by reaction-diffusion fronts. Experimentally, these fronts have been observed to be either isotropic or triangular depending on the conditions of preparation of the oxygen layer as well as on temperature and hydrogen pressure. If we model only the surface reaction and the diffusion of hydrogen, we obtain isotropic fronts with velocities in the range of $2-3\ \mu m\,s^{-1}$. These results are in line with experimental measurements for surfaces exposed to oxygen for a short period. To correctly reproduce the possible triangular shape of the titration fronts and the smaller front velocities of $0.1-1\ \mu m\,s^{-1}$ for experiments with the surface exposed to oxygen for a long time (>1 h), we have to include the formation of a subsurface oxygen-rich phase and its removal. It is assumed that the phase transition between the oxygen-rich and oxygen-free subsurface phases occurs via front propagation, and the front speed has triangular symmetry compatible with the symmetry of the crystalline bulk. By fitting parameters describing the propagation of the phase transition front, its anisotropy and its coupling to the reaction-diffusion front on the surface, we have been able to quantitatively reproduce all experimental observations presented by Schaak and Imbihl in Chem. Phys. Lett. **283**, 386 (1998). © *2002 American Institute of Physics.*
[DOI: 10.1063/1.1496481]

I. INTRODUCTION

Spontaneous formation of spatial structures and nonlinear waves is observed in chemical reactions in solution (homogeneous catalysis) as well as in surface reactions (heterogeneous catalysis).[1] While concentration patterns in the Belousov–Zhabotinsky and other homogeneously catalyzed liquid phase reactions were discovered already around 1970,[2] pattern formation in heterogeneous catalysis[3] has been studied systematically only after the arrival of the photoemission electron microscope (PEEM).[4] Surface catalysis has provided not only a truly two-dimensional system, but also introduced new aspects like anisotropy[5] and global coupling[6–8] into the field of pattern formation. Experiments have revealed square-shaped patterns[9,10] and traveling fragments[11] in the reaction of $NO+H_2$ on a Rh(110) surface and more recently triangular fronts[12] in the O_2+H_2 reaction on a Rh(111) surface as new phenomena due to anisotropy.

Square-shaped patterns[10,13–15] and traveling fragments[11] have been modeled with reaction-diffusion equations that contain anisotropic and coverage dependent diffusion coefficients. An analysis of a reaction-diffusion model with competing anisotropic diffusion processes led to the discovery of further novel phenomena including stratified spatiotemporal chaos[16] and suppression of labyrinthine patterns.[17] In all these models, diffusion is assumed to be anisotropic as a result of the anisotropy of the catalytic surface, e.g., the (110) surface. In contrast, surface diffusion is isotropic on the Rh(111) surface. Consequently, anisotropic surface diffusion is ruled out as an explanation for the triangular fronts which appear between patches of surface H resp. O and were reported in Ref. 12 (see Fig. 1).

In the latter work, a Rh(111) surface is covered with oxygen for a defined exposure time. Then, oxygen flow into the reaction chamber is closed and hydrogen is added with a constant gas phase pressure. This leads to a reactive removal of the oxygen by hydrogen (titration) and eventually to a hydrogen covered surface. A closer look at the experiment shows that triangular fronts only form after a sufficiently a long exposure of the sample to oxygen (>1 h), while for short exposure times, isotropic and much faster fronts are observed. Triangular fronts are seen for high hydrogen pressures or low temperatures. In addition, it is known that a subsurface oxygen layer is formed during front propagation in the O_2+H_2 reaction on Rh(111).[18] These experiments have been successfully modeled by a reaction-diffusion system that is based on the elementary steps of the surface reaction and allows a local exchange of oxygen between the adsorbed layer and a subsurface layer.[19] Subsurface oxygen also plays a role in pattern formation in the CO oxidation on Pt(110).[20,21]

Here, we propose a model that includes also the effect of subsurface oxygen on the propagation of the hydrogen front during the titration experiments.[12] The model is based on the mechanism of the surface reaction between oxygen and hy-

[a)]Also at: Minerva Center for Nonlinear Physics of Complex Systems, and Institute of Catalysis Science and Technology, Technion; 32000 Technion City, Haifa, Israel; electronic mail: pismen@tx.technion.ac.il

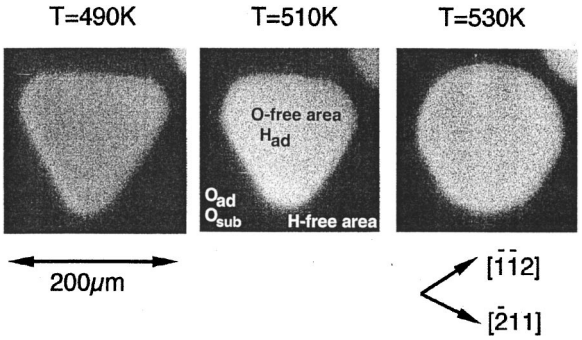

FIG. 1. PEEM images showing triangular and circular front geometries during the titration of the (8×8)-O structure on Rh(111) with hydrogen ($p_{H_2}=5.6\times10^{-7}$ mbar) at varying temperatures. (Reprinted from Ref. 12.)

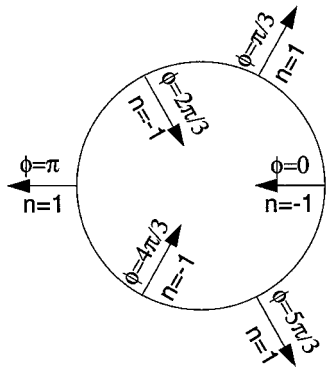

FIG. 3. Plot of the normal vector $n=-\cos 3\phi$ modeling the triangular anisotropy.

drogen that leads to water formation and hydrogen surface diffusion. It allows an exchange of oxygen between surface and bulk. We assume that a subsurface oxygen layer will form during the long exposure to oxygen. This subsurface oxygen-rich phase is removed during the titration and the phase transition to the pure bulk phase propagates via a phase transition front. The propagation of this front is affected by the microscopic structure and reflects the microscopic tetrahedron structure of the Rh crystal (see Fig. 2), while the surface diffusion of hydrogen occurs on a hexagonal lattice and is thus well described by an isotropic diffusion operator. We assume that as the subsurface oxygen rises to the surface it is influenced by the tetrahedral atomic structure in the crystal bulk. This causes the subsurface front to spread with different velocities depending on its orientation with respect to the crystal axes. The angular dependence of the front velocity obeys a triangular symmetry.

Altogether, our model describes the coupling between an isotropic reaction-diffusion process on the surface with an anisotropic phase transition front (with triangular symmetry) proceeding from the oxygen-rich to the pure phase in the subsurface layer. The coupling is mutual; the release of subsurface oxygen slows down the hydrogen titration front on the surface, while the phase transition front propagates only as a result of the subsurface transport towards the surface. The details of the model and its derivation will be described in Sec. II. In Sec. III, numerical simulations of the model in one and two dimensions are performed and compared in great detail to the experimental results.[12] While most rate constants for the adsorption of hydrogen and the reaction of hydrogen and oxygen are known from other experiments, assumptions on the speed of the phase transition front and the degree of anisotropy have to be made. The systematic experimental investigations of propagation speed of the hydrogen titration front on the surface and the degree of its anisotropy as a function of the control parameters—temperature and hydrogen pressure—allow us to fit these unknown parameters in the model. In general, we find that the slower front ''enslaves'' the faster one and characterizes the observed pattern. For high temperatures and low hydrogen pressures, isotropic patterns are observed, because then the titration front is slower than the phase transition front. For the opposite limits of control parameters, triangular patterns are found because the subsurface oxygen front slows down the titration front and imposes its triangular shape on it. In all cases, the front velocities are considerably smaller if the surface is pretreated with oxygen and a coupling to subsurface oxygen removal affects the titration process. This could be expected for the case where the subsurface front enslaves the hydrogen front on the surface, but comes as a surprise for the opposite case. A concise summary and discussion is given at the end of the article.

The proposed model shows that the microscopic symmetry of the crystal can affect reaction-diffusion fronts on the surface, provided that they are coupled to the removal of a bulk subsurface oxygen phase. This mechanism for the formation of patterns with broken rotational symmetry is qualitatively different from the impact of anisotropic surface diffusion on Rh(110) and Pt(110) reported in the past.

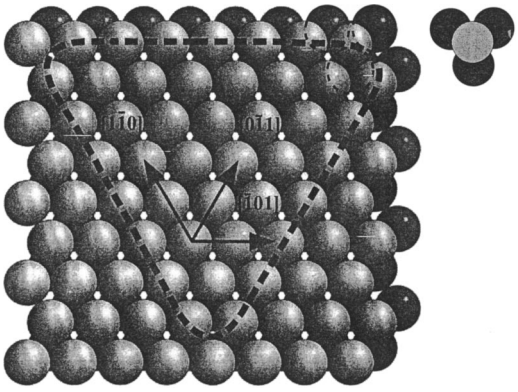

FIG. 2. Structural model of the two upper Rh(111) surface layers formed by a tetrahedron structure. (Reprinted from Ref. 12.)

II. THE MODEL

The proposed model is based on the kinetics of the hydrogen–oxygen reaction on a catalytic surface. The assumed reaction scheme for water formation reads[22]

$$H_2+2^*\rightarrow 2H_{ad},\quad O_2+2^*\rightarrow 2O_{ad},$$

$$O_{ad}+H_{ad}\rightarrow OH_{ad}+^*,\quad OH_{ad}+H_{ad}\rightarrow H_2O+2^*.$$

The reversible formation of subsurface oxygen is added

$$O_{ad} \rightleftharpoons O_{sub} + *.$$

For simplicity, we have neglected desorption processes. It is also assumed that the first step of the reaction, the formation of OH_{ad}, is the rate limiting step. During the titration process the rate of oxygen adsorption is zero. The concentration of subsurface oxygen is difficult to determine, since it is not known how deep oxygen penetrates into the bulk of the Rh crystal. Instead, we assume that there is a subsurface oxygen-rich phase in the bulk underneath a completely oxygen covered surface, given a long enough dosage of the oxygen before the titration. For short dosage times, only the surface is covered with oxygen and the bulk is in the pure Rh phase. If the surface oxygen is removed, the subsurface oxygen segregates to the surface.

Characterization of a subsurface oxygen layer as a *phase* with a definite crystalline symmetry (though possibly different from that of a bulk oxide) is supported both by x-ray photoelectron diffraction data[23] and computations by means of the density-functional theory.[24] These studies reveal anisotropic crystalline structure of the subsurface layer with three-fold symmetry, as well as the tendency to the agglomeration of the subsurface species. According to the interpretation of x-ray data,[23] subsurface oxygen atoms preferentially occupy octahedral sites between the first and second Rh layer, just underneath the face-centered cubic (fcc) surface adsorption sites. The theoretical study[24] concludes, however, that this configuration is metastable, whereas tetrahedral subsurface configuration is energetically favorable. Irrespectively to disagreement in crystallographic details, the subsurface phase acquires three-fold (triangular) symmetry, which is a consequence of the tetrahedral local structure of the fcc Rh crystal. It is qualitatively different from the six-fold (hexagonal) symmetry of a single layer forming a (111) crystal face.

It is clear that only the influence of the bulk crystalline structure may be responsible for surface patterns with a triangular symmetry, such as triangular titration fronts of hydrogen that remove surface oxygen observed in the experiment.[12] This symmetry is also observed, in particular, in triangular faceting patterns obtained in simulations of kinetically controlled crystal growth of fcc crystals.[25] A higher hexagonal symmetry in the (111) plane can be broken only due to bulk effects and, therefore, triangular symmetry is impossible as long as oxygen adsorbs on the surface and may arise when subsurface oxygen is present. This well agrees with the fact that triangular shapes were observed only following a long exposure to oxygen when subsurface absorption occurred.

In accordance with this, we base our model on the assumption that subsurface oxygen forms a *phase* separated from oxygen-free metal by a boundary, which possesses anisotropic line tension and is sharp when viewed on a macroscopic scale. When the surface adsorption layer is partially removed in the course of a titration experiment, a phase transition occurs, and the phase transition front propagates anisotropically, obeying a triangular symmetry in the (111) plane induced by the structure of the bulk phase. The front speed depends on the magnitude of the segregation flux, which, in turn, depends on the local surface concentration of the adsorbed species, and has triangular anisotropy compatible with the bulk structure.

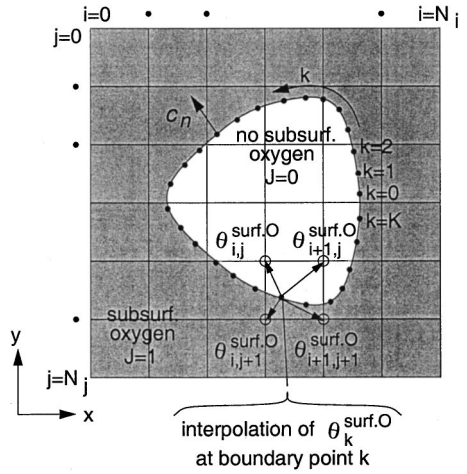

FIG. 4. The interphase boundary and surface grid.

Adding up all these ingredients, the model equations read

$$\frac{\partial \theta_H}{\partial t} = k_1 p_{H_2}\left(1 - \frac{\theta_O}{\theta_O^{sat}} - \theta_H\right)^2 - 2k_3\theta_O\theta_H + D_H\nabla^2\theta_H, \tag{1}$$

$$\frac{\partial \theta_O}{\partial t} = k_2 J(\theta_O^{sat} - \theta_O) - k_3\theta_O\theta_H, \tag{2}$$

where θ_O and θ_H are the surface concentrations of O_{ad} and H_{ad}, and J is a subsurface oxygen stepfunction:

$$J = \begin{cases} 1, & \text{for the phase with the subsurface oxygen} \\ 0, & \text{for the phase without the subsurface species.} \end{cases} \tag{3}$$

The expression for the angle-dependent speed $c_n(\phi)$ of the phase transition front is

$$c_n(\phi) = c_0(1 + \alpha_0 \cos 3\phi)(\theta_O^{sat} - \theta_O). \tag{4}$$

By our definition, the velocity is positive when the oxygen-free state advances (see Figs. 3 and 4). If we assume that the oxygen gradient $(\theta_O^{sat} - \theta_O)$ in the aforementioned formula is constant, we can apply the criterion for formation of sharp corners $c_n(\phi) + d^2c_n(\phi)/d\phi^2 < 0$ (compare Ref. 13) to the phase transition front. One easily finds that sharp corners form if $\alpha_0 > 1/8$. This relation implies that the ratio v of side-to-corner velocity fulfills $v = c_{side}/c_{corner} < 7/9 \approx 0.778$. This oversimplified argument is indeed in reasonable agreement with the measurements presented in Fig. 1; for the triangular shapes at $T = 490$ K resp. $T = 510$ K, experiments report $v = 0.70$ resp. $v = 0.73$, while $v = 0.85$ is measured for the weakly elliptic, almost isotropic titration front at $T = 530$ K. Below, we shall use $\alpha_0 = 0.2$, which is not only consistent with the experimental observations, but also implies a triangular phase transition front, under conditions when the coupling to the surface processes can be neglected.

The algorithm for the simulation combines the numerical solution of Eqs. (1) and (2) with Eq. (3) on a square grid with Lagrangian propagation of the phase transition front accord-

TABLE I. Basic constants of the model, $k_i = v_i^0 \exp(-E_i^a/RT)$.

k_i	Preexponential factor, v_i^0	Activation energy, E_i^a (kJ/mol)	Reference No.
H_2 adsorption, k_1	2.22×10^5 ML s^{-1} $mbar^{-1}$	···	26
oxygen transport, k_2	1×10^{13} s^{-1}	120	···
$H_{ad}+O_{ad}$ reaction, k_3	1×10^{13} ML^{-1} s^{-1}	110	26
H_{ad} diffusion, D_H	0.25 μm^2 s^{-1}	18	27
velocity, c_0	0.45×10^{13} μm s^{-1}	120	···

ing to Eq. (4). The details are presented in Appendix A. The results of the computations will be further compared in detail with the experimental data of the ratio between side and corner velocities of the titration fronts.[12]

III. NUMERICAL RESULTS

The parameter values used in the following computations are presented in Tables I and II. First, the simulations have been carried out in one dimension for different orientations ϕ in order to obtain the front speed dependence on T and p_{H_2} and estimate the parameters of Eq. (4). In this computation, $\nabla^2\theta_H$ in Eq. (1) is replaced by the second derivative $\partial^2\theta_H/\partial x^2$. In the simulation with $k_2=0$ (pure phase) the front propagates isotropically and fast. As seen in Fig. 5(a), the simulation somewhat underestimates the increase of the front speed with growing temperature. A possible reason is the neglected temperature dependence of the hydrogen sticking coefficient that enters the adsorption rate k_1: We have used the data from Ref. 26, where $k_1=$constant, while it is likely to be T activated. When the subsurface oxygen is included in the model, the front propagation is delayed significantly, and anisotropy is observed. Assuming triangular symmetry described by the angle-dependent function in Eq. (4), we need to compute the velocity of the "corner" and "side" fronts

$$c_n = c_0(1+\alpha_0 n)(\theta_O^{sat}-\theta_O), \quad \text{where} \begin{cases} n_{side}=-1, \\ n_{corner}=1. \end{cases} \tag{5}$$

The ratio c_{side}/c_{corner} will serve to indicate the anisotropy ($c_{side}/c_{corner}\approx1$ for the circular front and $c_{side}/c_{corner}<1$ for the triangular one). Since we have no data describing the nature of the $O_{sub}\rightarrow O_{ad}$ transition, the coefficients k_2, c_0, and α_0 have been fitted. The comparison of experiments with the simulations is shown in Figs. 5(b) and 5(c). Note, that the front velocities in the model with the subsurface oxygen phase in Fig. 5(b) are considerably lower than the velocity for the pure surface reaction with $k_2=0$ in Fig. 5(a). It is instructive to consider the change of the temperature dependent velocity coefficient c_0 that governs the speed of the phase transition. For $T=460$ K, we have $c_0\approx0.06$ μm s^{-1},

TABLE II. Other coefficients.

Coefficient	Value
Surface oxygen fraction at saturation, θ_O^{sat}	1
Anisotropy coefficient, α_0	0.2

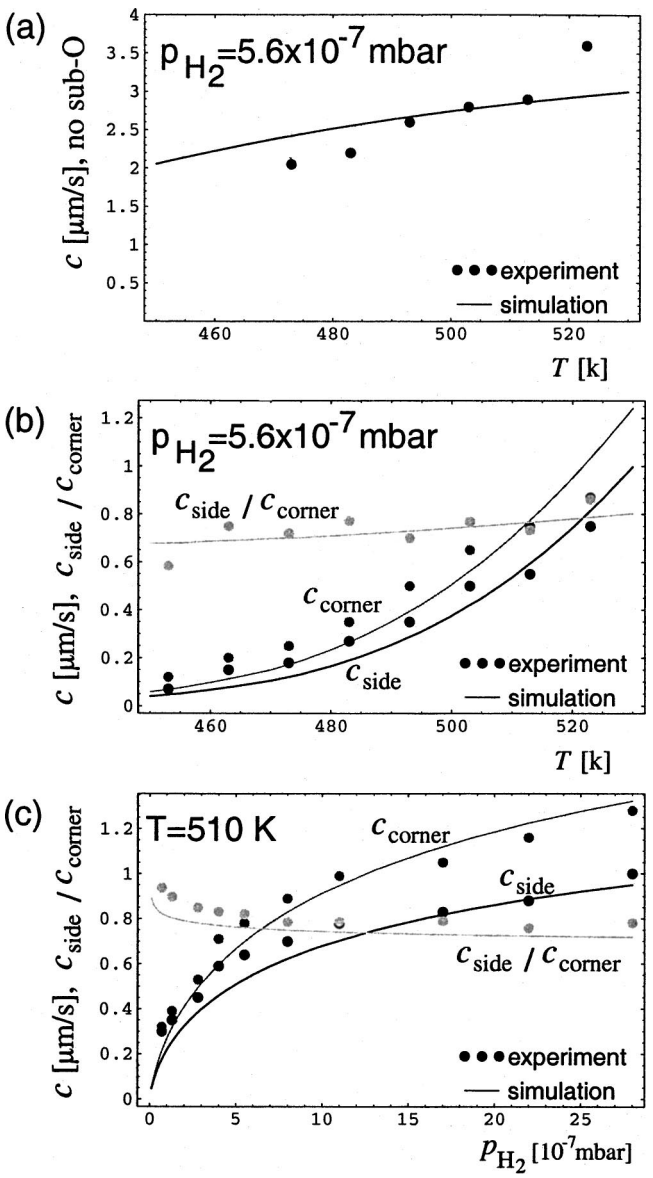

FIG. 5. Dependence of the front velocity on T and p_{H_2} for two differently prepared oxygen covered surfaces: nonoxidized (a) and oxidized surface [(b) and (c)].

whereas for $T=530$ K, one gets $c_0\approx7.44$ μm s^{-1}. Thus, the phase transition front is strongly temperature dependent, while the titration front in the case without subsurface oxygen is only weakly temperature dependent: it changes from ≈2.2 μm s^{-1} at $T=460$ K to ≈3.0 μm s^{-1} at $T=530$ K [see Fig. 5(a)]. These data also indicate that it is faster (slower) than the triangular phase transition front at low (high) temperatures. Interestingly, this change coincides with a change of the morphology from triangular to isotropic fronts if the two processes are coupled. From this, we can conclude that the slower front determines the morphology of both fronts in the case where both fronts are coupled.

The profiles of θ_H and θ_O in one-dimensinal (1D) simulations are shown in Fig. 6. At low T, the oxygen coverage at the front position is far from the saturation value 1 and hydrogen has penetrated the area where the oxygen-rich subsurface phase is present, while at high T, the oxygen cover-

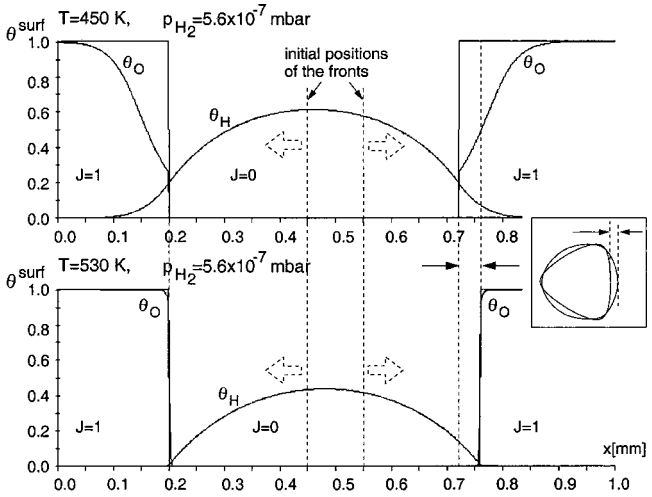

FIG. 6. Front profiles obtained in 1D simulations for different temperatures at constant hydrogen pressures, corresponding profiles from 2D simulations are almost indistinguishable. Inset: the final 2D shape at $T=450$ K (triangle) and $T=530$ K (circle).

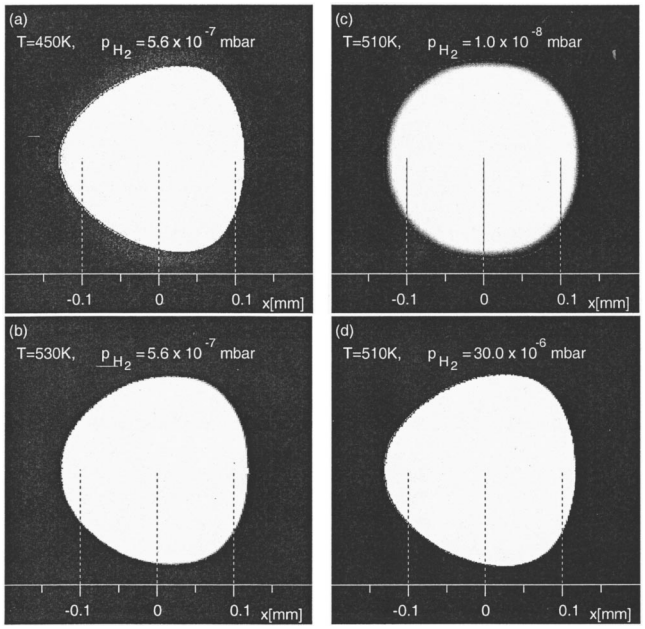

FIG. 8. 2D simulation of developing triangular shaped fronts at different conditions. The gray-scale images show surface oxygen distribution: $\theta_O=0$ inside the spots (white area) and $\theta_O=1$ outside (black area).

age at the front is close to unity and subsurface oxygen is practically absent beneath the area where hydrogen is adsorbed. These front shapes indicate that the visible and experimentally recorded surface titration front is slowed down and adjusts to the invisible phase transition front at low T, while it is itself slowing the phase transition front at high T, in line with the above reasoning. The front speed has been measured as a mean value of c_n. Despite the fact that the O-free part of the surface is still not saturated by hydrogen, the front speed can be assumed as ''stationary'' after the front passes a transient. The duration of this transient has been determined from numerical tests. An example of front speed relaxation is shown in Fig. 7.

The variation of the experimental conditions does not cause changes in the crystal anisotropy, i.e., the rate of the $O_{sub}\rightarrow O_{ad}$ transport (k_2) remains homogeneous over the entire surface. The anisotropy reveals itself due to reaction kinetics when the slow progress of the phase transition front (small k_2, D_{H_2} low T) delays the front propagation. Under these conditions, the anisotropy of the $O_{sub}\rightarrow O_{ad}$ transition is pronounced, and the front has the triangular shape (regime I). On the contrary, relatively faster progress of the phase transition front (big k_2, high T) is hindered by the slower titration front propagation, which then leads to a circular front shape (regime II). The hydrogen pressure accelerates the front velocity proportionally to $\sqrt{p_{H_2}}$.[28] This experimental observation is in agreement with the model results presented in Fig. 5(c). An increase of p_{H_2} causes fast propagation of the hydrogen front, then the phase transition has limiting effect (regime I), therefore, the front exhibits the triangular shape. At low p_{H_2}, the regime II is reproduced. Two-dimensional (2D) simulations are in a good agreement with the 1D calculations and experiments (see Figs. 1 and 8). A decrease of T and increase of p_{H_2} lead to a more pronounced anisotropy of propagating fronts, as seen in Fig. 8. The 1D sections of the 2D simulation results through the midside and corner (at $y=0$) almost coincide with 1D results.

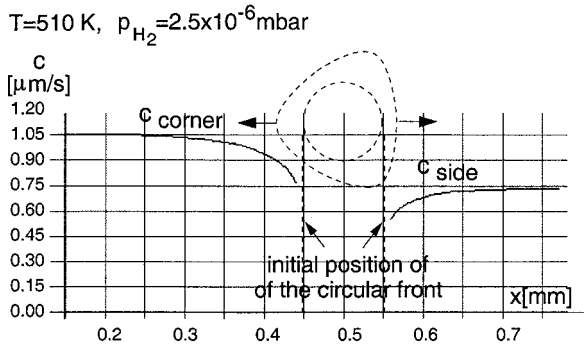

FIG. 7. The front speed transient affected by θ_H coverage. Insert: the original circular front shape and its transformation to the triangular one.

IV. CONCLUSIONS

We have introduced a model for triangular titration fronts in the hydrogen–oxygen reaction on Rh(111). The model comprises hydrogen adsorption, reaction of O and H and isotropic hydrogen surface diffusion. In addition, we had to take into account the formation of a subsurface oxygen-rich phase, flux of subsurface oxygen onto the oxygen-free-surface, and a triangular anisotropy of the propagation speed of the phase transition front between the oxygen-rich and oxygen-free subsurface phases.

Apart from the external control parameters—hydrogen pressure p_{H_2} and surface temperature T—the model contains the parameters describing the oxygen segregation between the subsurface phase and surface and the mean velocity as well as the anisotropy parameter for the phase transition front. The anisotropy parameter, i.e., the ratio between the side and corner velocity of the triangular phase transition front, has been estimated to be roughly 2/3 from the largest

observed anisotropy of the experimental titration fronts, see Ref. 12 and data reproduced in Fig. 5(c). The velocity coefficient c_0 in the aforementioned model equation is assumed to be thermally activated. It is proportional to the flow of oxygen from the bulk to the surface described by the rate constant k_2. When the temperature decreases or the hydrogen pressure increases, the phase transition front is much slower than the reaction-diffusion front on the surface, which is mostly driven by hydrogen diffusion. In this case, it enslaves the titration front on the surface and imposes its triangular shape upon the latter front. In the opposite case, the titration front restores the isotropy and dominates the phase transition front. Altogether, we find that if two fronts with different morphologies are coupled, the slower one preserves its shape. The relative magnitude of the respective velocities assigned to the phase transition front and the reaction-diffusion front on the surface in the uncoupled case leads to the change from triangular to isotropic titration front shapes reported in Ref. 12.

ACKNOWLEDGMENTS

This research has been supported by the German–Israeli Foundation (GIF). The authors thank Ronald Imbihl for fruitful discussions and providing experimental figures.

APPENDIX A: ALGORITHM

The computations have been carried out according to the following scheme (see also Fig. 4):

(1) Set the polygon of the front interface points (circle of radius r), define p_{H_2}, T and initial coverages at the grid nodes as follows: Inside the front interface: $\theta_{Oi,j}=0$, $\theta_{Hi,j}=0$; outside the front interface: $\theta_{Oi,j}=\theta_O^{sat}$, $\theta_{Hi,j}=0$.

(2) Update the subsurface oxygen matrix on the grid: $J_{i,j}=0$—inside the front, $J_{i,j}=1$—outside.

(3) Solve the partial differential equation for θ_H by means of an implicit scheme and the ordinary differential equation for θ_O by a fourth-order Runge–Kutta method. Boundary conditions: $\partial\theta_H/\partial x=0$, $\partial\theta_H/\partial y=0$.

(4) When the tag of the front interface points k runs from 0 to K, interpolate θ_{Ok} at the positions $\{x_k^{old}, y_k^{old}\}$, compute c_{nk} and update each k-point position of the front interface as:

$$x_k^{new}=x_k^{old}+n_{xk}c_{nk}\Delta t, \quad y_k^{new}=y_k^{old}+n_{yk}c_{nk}\Delta t,$$

where $n_{xk}^2+n_{yk}^2=1$.

(5) The boundary points are separated by distances $d_{k,k+1}$. Check the front interface: if $d_{min}<d_{k,k+1}<d_{max}$, go to step 5, otherwise, add/remove points of the front interface.

(6) Output: $\theta_{Hi,j}$, $\theta_{Oi,j}$, $J_{i,j}$, array of the front interface points $\{x_k, y_k\}$. Return to step 1.

[1] *Chemical Waves and Patterns*, edited by R. Kapral and K. Showalter (Kluwer, Dordrecht, 1994).
[2] A. N. Zaikin and A. M. Zhabotinsky, Nature (London) **225**, 535 (1970).
[3] R. Imbihl and G. Ertl, Chem. Rev. **95**, 697 (1995).
[4] S. Jakubith, A. von Oertzen, W. Engel, H. H. Rotermund, and G. Ertl, Phys. Rev. Lett. **65**, 3013 (1990).
[5] M. Bär, E. Meron, and C. Utzny, Chaos **12**, 204 (2002).
[6] M. Eiswirth, P. Möller, K. Wetzl, R. Imbihl, and G. Ertl, J. Chem. Phys. **90**, 510 (1989).
[7] F. Mertens, R. Imbihl, and A. S. Mikhailov, J. Chem. Phys. **101**, 9903 (1994).
[8] M. Falcke and H. Engel, J. Chem. Phys. **101**, 6255 (1994).
[9] F. Mertens and R. Imbihl, Nature (London) **370**, 124 (1994).
[10] N. Gottschalk, F. Mertens, M. Bär, M. Eiswirth, and R. Imbihl, Phys. Rev. Lett. **73**, 3483 (1994).
[11] F. Mertens, N. Gottschalk, M. Bär, M. Eiswirth, A. Mikhailov, and R. Imbihl, Phys. Rev. E **51**, 5193 (1995).
[12] A. Schaak and R. Imbihl, Chem. Phys. Lett. **283**, 386 (1998).
[13] A. S. Mikhailov, Phys. Rev. E **49**, 5875 (1994).
[14] A. Makeev and R. Imbihl, J. Chem. Phys. **113**, 3854 (2000).
[15] A. Makeev, M. Hinz, and R. Imbihl, J. Chem. Phys. **114**, 9083 (2001).
[16] M. Bär, A. Hagberg, E. Meron, and U. Thiele, Phys. Rev. Lett. **83**, 2664 (1999); Phys. Rev. E **62**, 366 (2000).
[17] E. Meron, M. Bär, A. Hagberg, and U. Thiele, Catal. Today **70**, 331 (2001).
[18] A. Schaak and R. Imbihl, J. Chem. Phys. **113**, 9822 (2000).
[19] M. Monine, A. Schaak, B. Y. Rubinstein, R. Imbihl, and L. M. Pismen, Catal. Today **70**, 321 (2001).
[20] A. von Oertzen, A. S. Mikhailov, H. H. Rotermund, and G. Ertl, J. Phys. Chem. B **102**, 4966 (1998).
[21] A. von Oertzen, H. H. Rotermund, A. S. Mikhailov, and G. Ertl, J. Phys. Chem. B **104**, 3155 (2000).
[22] V. P. Zhdanov, Surf. Sci. **296**, 261 (1993).
[23] J. Wider, T. Greber, E. Wetli, J. T. Kreutz, P. Schwaller, and J. Osterwalder, Surf. Sci. **417**, 301 (1998).
[24] M. V. Ganduglia-Pirovano, K. Reuter and M. Scheffler, Phys. Rev. B **65**, 245426 (2002).
[25] A. A. Golovin, S. H. Davis, and A. A. Nepomnyashchy, Phys. Rev. E **59**, 803 (1999).
[26] A. Makeev, M. M. Slinko, and N. M. H. Janssen, J. Chem. Phys. **105**, 7210 (1996).
[27] E. G. Seebauer, A. C. F. Kong, and L. D. Schmidt, J. Chem. Phys. **88**, 6597 (1988).
[28] A. Schaak, S. Shaikhutdinov, and R. Imbihl, Surf. Sci. **421**, 191 (1999).